Medical Image Analysis 97 (2024) 103225

Contents lists available at ScienceDirect

Medical Image Analysis

journal homepage: www.elsevier.com/locate/media

MMGPL: Multimodal Medical Data Analysis with Graph Prompt Learning

Liang Peng [a], Songyue Cai [b], Zongqian Wu [b], Huifang Shang [c], Xiaofeng Zhu [a,*], Xiaoxiao Li [d]

[a] Shenzhen Institute for Advanced Study, University of Electronic Science and Technology of China, Shenzhen 518000, China
[b] School of Computer Science and Engineering, University of Electronic Science and Technology of China, Chengdu 611731, China
[c] Department of Neurology, Laboratory of Neurodegenerative Disorders, National Clinical Research Center for Geriatrics, West China Hospital, Sichuan University, Chengdu 610041, China
[d] School of Electrical and Computer Engineering, University of British Columbia, Vancouver BC V6T 1Z4, Canada

ARTICLE INFO

Keywords:
Prompt learning
Multimodal models
Neurological disorders
Graph neural network

ABSTRACT

Prompt learning has demonstrated impressive efficacy in the fine-tuning of multimodal large models to a wide range of downstream tasks. Nonetheless, applying existing prompt learning methods for the diagnosis of neurological disorder still suffers from two issues: (i) existing methods typically treat all patches equally, despite the fact that only a small number of patches in neuroimaging are relevant to the disease, and (ii) they ignore the structural information inherent in the brain connection network which is crucial for understanding and diagnosing neurological disorders. To tackle these issues, we introduce a novel prompt learning model by learning graph prompts during the fine-tuning process of multimodal models for diagnosing neurological disorders. Specifically, we first leverage GPT-4 to obtain relevant disease concepts and compute semantic similarity between these concepts and all patches. Secondly, we reduce the weight of irrelevant patches according to the semantic similarity between each patch and disease-related concepts. Moreover, we construct a graph among tokens based on these concepts and employ a graph convolutional network layer to extract the structural information of the graph, which is used to prompt the pre-trained multimodal models for diagnosing neurological disorders. Extensive experiments demonstrate that our method achieves superior performance for neurological disorder diagnosis compared with state-of-the-art methods and validated by clinicians.

1. Introduction

Neurological disorders, including Autism Spectrum Disorder (ASD) (Lord et al., 2018) and Alzheimer's Disease (AD) (Scheltens et al., 2021), severely impair subjects' social, linguistic, and cognitive abilities, and have already become serious public health issues worldwide (Feigin et al., 2020). Unfortunately, there are no definitive cures for most neurological disorders (*e.g.,* ASD and AD), so the diagnosis of neurological disorder is urgently needed to promote early intervention and delay its deterioration (Wingo et al., 2021; Zhu et al., 2022). Over the last decade, researchers (Wen et al., 2020; Li et al., 2021; Dvornek et al., 2019) have applied various machine learning methods, such as Convolutional Neural Networks (CNN) (LeCun and Bengio, 1995), Graph Neural Networks (GNN) (Kipf and Welling, 2017), and Recurrent Neural Networks (RNN) (Schuster and Paliwal, 1997), to diagnose neurological disorders. Despite the remarkable progress made by these methods, the robustness and effectiveness of these deep learning models are difficult to ensure due to the fact that these methods are directly trained on small-scale and complex medical datasets (Dinsdale et al., 2022).

Recently, multimodal large models (Liu et al., 2023; Driess et al., 2023; Tu et al., 2023; Wu et al., 2023) with extensive parameters, trained on vast datasets and diverse tasks, have exhibited remarkable generality and adaptability. As a result, multimodal large models have become a recent focal point within the field of medical data analysis. Researchers across various domains have developed disparate products such as the large language models (*e.g.,* GPT (OpenAI, 2023)) and the large vision models (*e.g.,* SAM (Kirillov et al., 2023)). They can accelerate the development of accurate and robust models, reducing reliance on extensive labeled data (Zhang and Metaxas, 2023). Owing to their generality, multimodal large models hold immense potential in addressing a wide array of diagnostic tasks for neurological disorders.

However, applying these multimodal large models in the field of neurological disorders diagnosis faces significant challenges due to the diverse modalities in multimodal medical data (*e.g.,* PET and MRI), which differ greatly from natural images. To fill the gap between the pre-training tasks and downstream tasks, researchers utilize techniques such as full fine-tuning and prompt learning on pre-trained multimodal large models to address specific downstream tasks in medicine domains.

[*] Corresponding author.
E-mail address: seanzhuxf@gmail.com (X. Zhu).

https://doi.org/10.1016/j.media.2024.103225
Received 16 December 2023; Received in revised form 12 April 2024; Accepted 27 May 2024
Available online 28 May 2024
1361-8415/Crown Copyright © 2024 Published by Elsevier B.V. All rights are reserved, including those for text and data mining, AI training, and similar technologies.

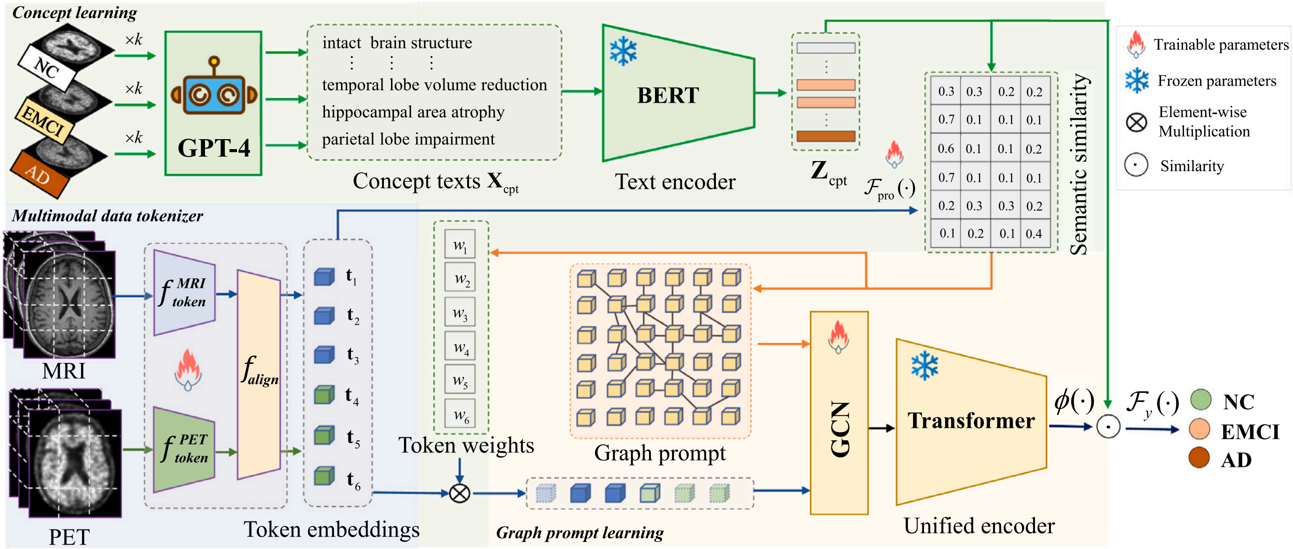

0.3	0.3	0.2	0.2
0.7	0.1	0.1	0.1
0.6	0.1	0.1	0.2
0.7	0.1	0.1	0.1
0.2	0.3	0.3	0.2
0.1	0.2	0.1	0.4

Fig. 1. The flowchart of the proposed MMGPL consists of three modules *i.e.,* multimodal data tokenizer (light blue block), concept learning (light green block), and graph prompt learning (light yellow block). First, MMGPL divides the multimodal medical data into multiple patches and project them into a shared embedding space (Section 3.2). Second, MMGPL prompts the GPT-4 to generate disease-related concepts and further learn the weights of tokens based on the semantic similarity between tokens and concepts (Section 3.3). Third, MMGPL learns a graph among tokens and extracts structural information to prompt the unified encoder (Section 3.4). Finally, MMGPL obtains the output from the unified encoder and uses it to predict the label of the subject.

Specifically, full fine-tuning is a commonly used method in transfer learning, which updates the weights of pre-trained models on task-specific data. However, full fine-tuning methods (Howard and Ruder, 2018) are becoming increasingly difficult to operate when dealing with large models with massive parameters because they require fine-tuning the entire model directly. Recently, prompt learning (Brown et al., 2020) has become a new fine-tuning paradigm of modern multimodal large models, which explicit instructions or adjusts only a small portion of parameters of prompts to guide the foundation model. For example, Lester et al. (2021) demonstrates that even for models of the 10 billion parameter scale, optimizing the prompt alone while keeping the model parameters fixed can achieve performance comparable to that of full fine-tuning.

Despite the impressive results demonstrated by prompt learning, it is highly task-specific, requiring researchers from different domains to design customized prompts to maximize its potential. In the field of Natural Language Processing (NLP), previous works usually employed cloze prompts, which can be designed manually or automatically. For example, Brown et al. (2020) manually defines specific prompt templates to boost various NLP tasks. However, manually adjusting the prompt templates lacks flexibility and efficiency. To yield more flexible and efficient prompts, some researchers (Lu et al., 2022; Gao et al., 2020; Schick and Schütze, 2020) proposed to discover prompts through automatic learning under supervised data. Inspired by the successful application of prompt learning in NLP, researchers have started exploring prompt learning in computer vision (CV). For instance, VPT (Jia et al., 2022) proposed a single-modality prompt learning method that designs individual prompts for images. However, the single-modality prompt learning method only prompts one modality and ignores the prompt from the other modality. To yield more effective prompt learning, Khattak et al. (2023) and Zhou et al. (2022) designed to prompt both image modality and text modality. Despite the widespread application of prompt learning methods in the fields of NLP and CV, we still face challenges when applying prompt learning to fill the gap between the pre-training multimodal large models and the diagnosis of neurological disorders.

Firstly, only a small fraction of patches in neural data are related to the disease. Unlike natural image data, the pathological regions or the regions of interests (*i.e.,* ROIs) in neural data typically only occupy a small portion of the entire data. For example, previous studies (Paduraríu et al., 2012; Wang et al., 2006) have shown a significant correlation between the hippocampal area and Alzheimer's disease. Recently, in the field of medical image segmentation, researchers (Huang et al., 2023; Zhang et al., 2023c) explored region-based prompts, such as bounding boxes and clicks, to guide the large vision model focus on the relevant areas of the medical images. Despite the promising results obtained by region-based prompts, the aforementioned operations (*e.g.,* bounding box and clicks) often rely on human interaction or object detection models which reduces the flexibility of these methods. Moreover, implementing the aforementioned operations becomes even more challenging when dealing with multimodality neural data, which may typically contains 3D tensor MRI data, time-series data, and functional connectivity (FC) network data. Hence, it is challenging to discover useful patches when dealing with multimodality neural data.

Secondly, the structural information among patches plays a crucial role in the analysis of neurological disorders. In the field of neuroscience, researchers (Bullmore and Sporns, 2009; Fornito et al., 2015) have indicated that the brain is a complex and interconnected network/graph, and the connection topology (*i.e.,* structural information) of the brain fundamentally shapes the progression of neurological disorders. Although the transformer architecture includes a graph block (*i.e.,* composed of keys, queries, and values) for extracting global patterns, its dense nature (Jaszczur et al., 2021) makes the model difficult to capture the structural information among patches. Additionally, the model parameters are fixed in prompt-based fine-tuning, which means that the structural information learned through key-query weights may not suitably represent the structural information relevant to neurological disorders. Thus, it is essential to extract structural information among patches in prompt learning for the diagnosis of neurological disorders.

To address the aforementioned challenges, we propose MMGPL: *Multimodal Medical Data Analysis with Graph Prompt Learning*. The proposed method is a prompt-driven multimodal medical model for the diagnosis of neurological disorders. As shown in Fig. 1, the proposed MMGPL consists three modules, *i.e.,* multimodal data tokenizer (Section 3.2), concept learning (Section 3.3), and graph prompt learning (Section 3.4). Firstly, we employ multimodal data tokenizer which projects all modalities into a shared token space. This allows MMGPL to efficiently handle multimodal medical data. Secondly, we leverage a general artificial intelligence model (GPT-4) (OpenAI, 2023) to automatically obtain disease-related concepts (Koh et al., 2020) and further embed these concepts. Additionally, each token (patch embedding) will be compared to all concepts for similarity, and the weight of the patch will be calculated based on the token's similarity to its corresponding category concepts. As a result, it addresses the first challenge by handling irrelevant patches. Thirdly, we learn the graph structure among patches based on their relationships with concepts. As a result, it tackles the second challenge by inputting the learned graph structure and the embeddings of corresponding tokens as inputs to a Graph Convolutional Network (GCN) (Kipf and Welling, 2017). This allows for the propagation of structural information among patches, enhancing the overall understanding of the connection between different brain regions. To this end, the new embeddings of tokens are fed into the pre-trained unified encoder to obtain the representation of each subject.

Compared to previous methods, the main contributions of our method are summarized as follows.

- We introduce a novel prompt learning method that effectively reduces the impact of irrelevant patches, which is usually overlooked in existing methods but is crucial in medical data analysis.
- Our method innovatively employs a graph prompt to extract structural information among patches. To the best of our knowledge, this is the first attempt to design prompt learning methods with a focus on the pathogenesis of neurological diseases, thereby bridging the gap between multimodal models and neurological disease diagnosis. Further, MMGPL demonstrates effectiveness across multiple neurological disease datasets and exhibits excellent scalability and flexibility, making it a promising solution for handling multimodal data in the diagnosis of neurological diseases.

2. Related works

2.1. Multimodal large models

Unlike traditional large language models such as GPT-3 (Brown et al., 2020) and BERT (Devlin et al., 2018), which can only deal with text data, multimodal large models (Radford et al., 2021; Tsimpoukelli et al., 2021; Liu et al., 2023; Driess et al., 2023) can integrate multiple modalities, such as language, vision, and audio, to perform a broad spectrum of tasks. For instance, CLIP (Radford et al., 2021) leverages a contrastive learning approach for joint pre-training on image–text pairs data. Besides, LLaVA (Liu et al., 2023) conducts image–text representation alignment followed by instruction tuning. Frozen (Tsimpoukelli et al., 2021) firstly proposed an approach that employs large language models in multimodal in-context learning. Similarly, Video-ChatGPT (Maaz et al., 2023) merges a video-adapted visual encoder with a large language model to handle video data. Recent works like Imagebind (Girdhar et al., 2023) and Meta-transformer (Zhang et al., 2023b) can learn a joint embedding across more than six different modalities.

In the medical domain, both large language models and multimodal large models have been recently explored for a wide range of medical tasks, including medical question answering and segmentation. For example, LLaVA-Med (Li et al., 2023) trains a vision-language conversational assistant research questions about medical images. Med-SAM (Ma and Wang, 2023) fine-tune the segment anything model (SAM) (Kirillov et al., 2023) on medical image data for segmentation task. Moreover, Med-PaLM (Tu et al., 2023) and RedFM (Wu et al., 2023) interpret multimodal biomedical data and handle a diverse range of tasks, moving closer to generalist medical artificial intelligence models. To incorporate a large-scale multimodal dataset, Zheng et al. (2023) build up a large-scale diagnostic dataset comprising 39,026 cases and 192,675 medical images. They utilized this dataset to train a powerful multimodal medical foundation model. To ensure the trustworthiness of large models, Sun et al. (2024) introduce principles for different dimensions of trustworthiness. However, due to the complexity of multimodal neuroimaging data, there is still a lack of research and remain challenges in leveraging multimodal large models for diagnosing neurological disorders.

2.2. Prompt learning

Prompt learning has emerged as a new paradigm in fine-turning pre-trained large models for various downstream tasks. Compared to full fine-tuning, it achieves comparable performance without updating all parameters in large models. In the field of NLP, GPT-3 (Brown et al., 2020) has demonstrated strong generalization to downstream tasks by manually selecting prompt texts. To improve the construction of prompt texts, Prefix-tuning (Li and Liang, 2021) optimizes prompts through gradient-based fine-tuning. In computer vision, VPT (Jia et al., 2022) prompts the image for effectively using the pre-trained image encoder in the classification task. SAM (Kirillov et al., 2023) takes visual prompts by drawing points, boxes, and strokes on an image for image segmentation. Moreover, MaPLe (Khattak et al., 2023) utilizes multi-modal prompts to guide models in both image and text modalities. Besides, Miyai et al. (2024) apply prompt learning for few-shot out-of-distribution detection.

In the field of medicine, prompt learning aims to guide models by focusing their attention on relevant regions within complex medical datasets. For example, several researchers (Ma and Wang, 2023; Huang et al., 2023; Zhang et al., 2023c) have introduced prompts such as bounding boxes and clicks into the SAM model to adapt it for medical image segmentation tasks. However, these methods may not be suitable for diagnosing neurological disorders given that they rely on human interaction or object detection models, as well as they do not take into account the importance of brain connectivity in neurological disorders.

2.3. Graph neural network

In the past decade, Graph Neural Networks (GNNs) have been widely used in computer-aided diagnosis (Sun et al., 2020; Bessadok et al., 2022; Holzinger et al., 2021; Li et al., 2021). GNNs such as Graph Convolutional Network (GCN) (Kipf and Welling, 2017) and Graph Attention Network (GAT) (Veličković et al., 2017) leverage message passing mechanism to capture relationships between nodes and structure information in the graph. Based on this, GNNs have the capability to leverage the inherent relationships between brain regions to uncover patterns or biomarkers associated with neurological disorder. As a result, there has been a growing interest in applying GNNs in the field of neuroscience (Li et al., 2021). For example, Parisot et al. (2018) exploits the GCN for Alzheimer's disease diagnosis in a population graph where the nodes in the graph denote the subjects and edges represent the similarity between subjects. Similarly, Kazi et al. (2019) proposes a GCN model with multiple filter kernel sizes on a population graph. Besides, Xu et al. (2023) leveraged graph structure information for biomedical synonym prediction. In addition, brain graph is also frequently used in the diagnosis of neurological disorders, where the nodes correspond to anatomical brain regions and the edges depict functional or structural connections between these regions. For instance, Li et al. (2021) conduct an interpretable model on brain graph to determine the specific brain regions that are associated with a particular neurological disorder. Cai et al. (2022) propose a transformer-based geometric learning approach to handle multimodal brain graphs for brain age estimation. However, there is still a lack of research on how to effectively leverage graph in multimodal models.

3. Methods

3.1. Preliminary and motivations

Utilizing transformers (Vaswani et al., 2017) as the architecture of encoders to process multimodal data has become a popular choice in modern multimodal large models, as it can effectively integrate information from multiple modalities. For example, pre-trained vision-language models like CLIP (Radford et al., 2021) employ separate transformer-based backbones (*e.g.,* ViT) to encode images and text separately. To obtain representations of the samples, the transformer architecture involves two key components: (i) Tokenization: converting the raw data into tokens. (ii) Encoding: performing attention-based feature extraction layers on all tokens.

Tokenization. The raw data from each modality is first tokenized into a sequence of tokens. Given an image input $\mathbf{X}$, the raw pixel data is typically partied into a set of patches $\mathbf{X} = \{\mathbf{x}_1, \mathbf{x}_2, \dots, \mathbf{x}_m\}$ where m is the number of patches, and each patch is flattened and projected into a token embedding $\mathbf{P} = \{\mathbf{p}_1, \mathbf{p}_2, \dots, \mathbf{p}_m\}$, which can be formalized as follows:

$$\mathbf{p}_i = \mathcal{F}(\mathbf{x}_i) + \mathbf{E}_i^{\text{pos}}, \quad \mathbf{p}_i \in \mathbb{R}^D \tag{1}$$

where $\mathcal{F}$ is a learnable projection function, D the dimensionality of token embedding, and $\mathbf{E}_i^{\text{pos}}$ is a positional embedding vector that encodes the location of ith patch within the image.

Encoding. The next step is to process the sequence of token embeddings through the Transformer's encoding layers. Each encoding layer consists of a multi-head self-attention (MHSA) layer followed by an MLP block. The encoding process in lth layer can be represented as:

$$\begin{aligned} \mathbf{H}^{(l)} &= \text{MHSA}(\text{LN}(\mathbf{Z}^{(l-1)})) + \mathbf{Z}^{(l-1)} \\ \mathbf{Z}^{(l)} &= \text{MLP}(\text{LN}(\mathbf{H}^{(l)})) + \mathbf{H}^{(l)}, \end{aligned} \tag{2}$$

where LN$(\cdot)$ is layer normalization operation, $\mathbf{Z}^{(l-1)}$ is the output from the previous layer and the input token embeddings for $l = 1$. In the MHSA layer, the attention mechanism computes multiple attention scores by performing dot products between the Query and Key vectors of the tokens, which represent dense interactions among tokens. A single-head attention operation can be expressed as follows:

$$\text{Attention}(\mathbf{Q}, \mathbf{K}, \mathbf{V}) = \text{softmax}\left(\frac{\mathbf{Q}\mathbf{K}^T}{\sqrt{d_k}}\right)\mathbf{V}, \tag{3}$$

where $\mathbf{Q}$, $\mathbf{K}$, and $\mathbf{V}$ are the query, key, and value vectors, respectively, and d_k is the dimensionality of the Key vectors, used for scaling. The softmax function is applied row-wise.

Prompt. Prompts can be used to adapt the pre-trained multimodal large models for various tasks without fully fine-tuning the model's parameters, which can be constructed through manual design or parameter learning (Brown et al., 2020; Gao et al., 2020). The prompt embeddings $\mathbf{P}_{\text{prompt}}$ are integrated with the input token embeddings $\mathbf{P}$:

$$\mathbf{P}_{\text{combined}} = \mathcal{F}_{\text{combine}}(\mathbf{P}_{\text{prompt}}, \mathbf{P}), \tag{4}$$

where $\mathcal{F}_{\text{combine}}$ denotes a fusion layer that can be a non-parametric operator ($\oplus$ or $+$) or parameterized layers. The combined token embeddings $\mathbf{P}_{\text{combined}}$ are subsequently processed by the transformer encoder, as delineated in Eq. (2). Based on this, previous methods proposed cross-modality prompt learning (Khattak et al., 2023) and deep prompt learning (Liu et al., 2022) to further improve its performance on specific tasks

However, previous methods face two challenges when applied to multimodal neural data: (i). Existing prompt learning methods usually overlook the impact of irrelevant patches. In the study of neural disorders, only a few patches in neural images are pertinent to the disease, which means the majority of tokens in $\{\mathbf{p}_1, \mathbf{p}_2, \dots, \mathbf{p}_m\}$ represent background information. However, all tokens are treated equally and interact with each other according to Eqs. (2) and (3), thereby limiting their effectiveness. (ii). Existing prompt learning methods have not taken into account the structural information among patches as indicated by Eq. (4). In the field of neuroscience, the intricate network structure of the brain plays a fundamental role in understanding neurological conditions. This highlights the significance of developing advanced methods that can effectively extract and utilize structural information for the diagnosis of neurological disorders. As a result, the performance of previous methods in the diagnosis of neurological disorders remains suboptimal.

In this paper, we propose a new prompt learning method to address the aforementioned challenges, and the framework is shown in Fig. 1. Specifically, we first perform a multimodal data tokenizer in Section 3.2 to project the raw data from different modalities into a shard token space, and then design the concept learning for tokens in Section 3.3 and the graph prompt learning in Section 3.4 to address the above issues.

3.2. *Multimodal data tokenizer*

Medical data is inherently multimodal, usually including modalities like MRI, PET, and FC in neurological disorder diagnosis. These diverse modalities provide complementary information, helping to gain a more comprehensive understanding and better analyze neurological disorders. However, these modalities often exhibit more complex data structures compared to natural images, such as 3D tensor medical data, brain connectivity graphs data, and time series data. Previous multimodal models like CLIP (Radford et al., 2021) handle text and images by employing distinct tokenizers and encoders for each modality. However, those methods may encounter challenges in terms of efficiency and scalability when dealing with multimodal medical data. Additionally, maintaining separate tokenizers and encoders for each modality is inflexible. Inspired by Meta-transformer (Zhang et al., 2023b) and Imagebind (Girdhar et al., 2023), we employ a multimodal data tokenizer that converts various multimodal medical data into token embeddings. Due to extensive research on the conversion of 2D image data (*e.g.,* X-ray and CT) and text data into tokens, there has been relatively less focus on tokenizing 3D tensor medical data (*e.g.,* MRI and PET). Therefore, in the following section, we focus on transforming 3D tensor medical data into tokens.

3.2.1. *Patch partitioning*

Specifically, for 3D tensor medical data (*e.g.,* MRI and PET), let us denote the raw data from M modalities as $\mathbf{X} = \{\mathbf{X}^1, \mathbf{X}^2, \dots, \mathbf{X}^M\}$, where each $\mathbf{X}^m \in \mathbb{R}^{H_m \times W_m \times D_m \times C_m}$ represents a distinct modality with its respective height H_m, width W_m, depth D_m, and number of channels C_m. For each modality m, we initiate the tokenization process by dividing the data into a set of patches $\mathcal{P}^m = \{\mathbf{p}_1^m, \mathbf{p}_2^m, \dots, \mathbf{p}_{N_m}^m\}$. where $\mathbf{p}_i^m \in \mathbb{R}^{S^3 \cdot C_m}$ is the ith patch, S is the uniform size of each patch in all dimensions, and $N_m = \frac{H_m W_m D_m}{S^3}$ is the total number of patches for m+th modality.

There are multiple approaches to dividing the data into a set of patches, including (i) 2D slice patch: each volumetric scan is sliced along one dimension, and each 2D slice is then partied into patches of size $S \times S$. The advantage of this approach lies in the fact that multimodal large models are typically pre-trained on 2D images, making it easier to transfer them to 2D medical images. However, this approach will generate a large number of tokens, which increases the computational and makes it more challenging to optimize. (ii) 2D axial slice patch: slices are taken along the axial plane, which is parallel to the plane of the 3D tensor's horizon, and each slice is divided into patches of size $S \times S$. The advantage of this approach is that it generates a considerable number of tokens. However, one drawback is that it can result in information loss. (iii) 3D patch: the 3D tensor data is divided into smaller cubes, with each cube being of size $S \times S \times S$. The advantage of this approach is that it generates a considerable number of tokens without causing information loss. However, one drawback is that it may contain gaps between tokens and the pre-training fundamental models. Note that, each approach has its advantages and disadvantages. Therefore, it is necessary to choose the most suitable method based on the specific task and characteristics of the data.

3.2.2. Tokenization

Each patch $\mathbf{p}_i^m$ is then transformed into a token through a modality-specific patch projection layer $\mathcal{F}_{\text{token}}^m$ and align the dimensions of the token embeddings from each modality, which can be expressed as follows:

$$\mathbf{t}_i^m = \mathcal{F}_{\text{token}}^m(\mathbf{p}_i^m) + \mathbf{E}_i^{m,\text{pos}}, \tag{5}$$

where $\mathbf{E}_i^{m,\text{pos}}$ is the position embedding of each patch in mth modality and the modality-specific patch projection layer $\mathcal{F}_{\text{token}}^m$ maps each patch $\mathbf{p}_i^m$ into a D-dimensional token embedding $\mathbf{t}_i^m$. As a result, we obtain all tokens from different modalities, *i.e.,* $\mathbf{T}^m = \{\mathbf{t}_1^m, \mathbf{t}_2^m, \dots, \mathbf{t}_{N_m}^m\}$.

We further project token embedding from multiple modalities into a shared token embedding space by a common learnable liner projection layer, which can be formalized as:

$$\mathbf{t}_i^m = \mathcal{F}_{\text{align}}(\mathbf{t}_i^m) + \mathbf{E}_{\text{modality}}^m, \tag{6}$$

where $\mathbf{E}_{\text{modality}}^m$ is the position embedding of each modality and $\mathcal{F}_{\text{align}}$ a common learnable liner projection layer. As a result, we obtain all tokens from all modalities, *i.e.,* $\mathbf{T} = \{\mathbf{t}_1, \mathbf{t}_2, \dots, \mathbf{t}_N\}$.

3.3. Concept learning

Once all token embeddings are obtained, it is crucial to consider the importance of each token because only a small fraction of tokens are related to the disease. However, it is challenging to identify these disease-related tokens due to the lack of annotations and the high dimensionality of tokens. To address this challenge, we propose to utilize concepts (Koh et al., 2020) of disease and compute the semantic similarity between each token and all concepts. We further reduce the weight or importance of irrelevant tokens according to the semantic similarity between each token and disease-related concepts.

3.3.1. Concept generation

Instead of providing low-level semantic information from the patches, the concepts refer to abstracting meaningful patterns from the data (Wang et al., 2023), thereby offering higher-level information that connects the patches to specific categories. In neurological disorders diagnosis, concepts are usually related to disease-specific information, such as symptoms, biomarkers, or radiological characteristics.

A straightforward approach to generating a set of concepts for diagnosing neurological disorders is to leverage human expertise. Handcrafting a set of concepts offers better interpretability as they align with human perception and understanding (Wang et al., 2023). However, it is important to note that the process of annotating these concepts can be costly, as well as requiring rich medical expertise. To avoid those issues, previous methods attempted to use GPT-4 (OpenAI, 2023) or other large language modal to generate concept texts. For example, Yang et al. (2023) proposed to prompt the large language model (*i.e.,* GPT-3) to generate candidate concepts. Based on this, Yan et al. (2023) proposed to elicit medical knowledge from GPT-4 to build a set of concepts for interpretable medical image classifiers. Thus, building concepts from large language models (*e.g.,* GPT-3 and GPT-4) has been success applied. In this study, we use GPT-4 to automatically generate the diseases-related concepts. Specifically, by prompting GPT-4 with specific instructions, we can generate lists of concepts that are typically associated with diseases, *e.g.,* "*Reduced Brain Metabolism: Individuals with AD typically exhibit slowed metabolic activity in the brain, particularly in the frontal and temporal lobes*". This approach reduces the annotation cost and leverages the capabilities of multimodal large models to generate concepts based on vast amounts of medical knowledge. More specifically, for C categories in specific neurological disorder diagnoses, we generate K relevant concepts for each category, which can be formalized as:

$$\mathbf{X}_{\text{cpt}} = \mathbf{GPT}(\{\text{CLS}_1, \text{CLS}_2, \dots, \text{CLS}_C\}, K), \tag{7}$$

where **GPT** denotes GPT-4 API (OpenAI, 2023), CLS denotes the name of corresponding category, and $\mathbf{X}_{\text{cpt}}$ denotes the generated text corresponding to $C \times K$ concepts. In this study, the concept texts have been validated by clinicians to ensure they are correct.

3.3.2. Semantic similarity computation

The obtained concepts are utilized to calculate the semantic similarity between each token t_i, and the disease-related concepts. This process assists in identifying the most pertinent tokens and adjusting their weights accordingly. As a result, it prompts the model to focus on important tokens, reducing interference from irrelevant tokens. To achieve this, we first input the text of concepts $\mathbf{X}_{\text{cpt}}$ with its corresponding category name into the text encoder $\mathcal{F}_{\text{text}}(\cdot)$ to obtain embeddings of concepts $\mathbf{Z}_{\text{cpt}}$, *i.e.,*

$$\mathbf{Z}_{\text{cpt}}^{c,k} = \mathcal{F}_{\text{text}}(\{\mathbf{X}_{\text{cpt}}^{c,k}, \text{CLS}_c\}), \tag{8}$$

where $\mathbf{Z}_{\text{cpt}}^{c,k}$ denote the final embedding of kth concept in cth category. Note that, the text encoder $\mathcal{F}_{\text{text}}(\cdot)$ and the tokenizer encoder have not pre-trained on paired data, so the distributions of $\mathbf{Z}_{\text{cpt}}$ and $\mathbf{T}$ are not aligned. Thus, we apply a learnable projection layer $\mathcal{F}_{\text{pro}}(\cdot)$ on tokens $\mathbf{T}$ to align their distributions. Next, we calculate the semantic similarity between tokens and concepts, *i.e.,*

$$\mathbf{s}_{i,c} = \frac{\exp(\text{sim}(\mathcal{F}_{\text{pro}}(\mathbf{t}_i), \mathbf{Z}_{\text{cpt}}^c)/\tau)}{\sum_{j=1}^{C\times K}\exp(\text{sim}(\mathcal{F}_{\text{pro}}(\mathbf{t}_i), \mathbf{Z}_{\text{cpt}}^j)/\tau)}, \tag{9}$$

where $\text{sim}(\cdot,\cdot)$ denotes the cosine similarity operator and τ denotes temperature parameter. After that, we calculate the weights of the tokens based on their relevance to the category-related concepts by:

$$w_i = \frac{\sum_{j\in C_i}\mathbf{s}_{i,j}}{\sum_{j=1}^{C\times K}\mathbf{s}_{i,j}} \times C, \tag{10}$$

where C_i is the set of concepts belonging to the category of this subject. Finally, we adjust the weight of the tokens and obtain the weight token embedding, *i.e.,* $\tilde{t}_i = w_i t_i$. Note that, as the category of the sample is unknown, we select C_i belongs to which set of concepts with the highest weight during the inference.

Finally, we adjust the weights of the tokens based on their relevance to the category-related concepts. Tokens with higher weights are deemed more pertinent in subsequent processing. This process helps the model to focus on the most relevant tokens and reduces the noise from irrelevant tokens. In addition, it is also necessary to consider the pathogenesis and biomarkers of neurological disorders when designing prompts.

3.4. Graph prompt learning

Neuroscience researchers (Rubinov and Sporns, 2010; Belmonte et al., 2004) have elucidated that the brain constitutes a complex graph structure, comprised of brain regions. The structural information of this graph, specifically the pattern of its connections, is crucial in the pathogenesis of neurological disorders. For example, deterioration and abnormal connectivity are candidate biomarkers for Alzheimer's disease (Pievani et al., 2014). Hence, the implementation of graph prompts is both reasonable and necessary for improving the ability of pre-trained multimodal large models to tackle the diagnosis of neurological disorders. To achieve this, we first construct the graph, and then extract embeddings from the constructed graph.

3.4.1. Graph construction

Considering that each token represents embedding of its corresponding patch (*i.e.,* local brain region), we first regard the tokens as nodes in the graph. Then, we construct the edges/graph structural $\mathbf{A}$ based on semantic relationships between tokens. Notably, directly calculating the relationships between tokens based on token embeddings $\mathbf{T}$ may not be the optimal choice since token embeddings $\mathbf{T}$ may contain limited information about disease-related information. To solve this issue, we leverage the concept embeddings obtained in Section 3.3 as the bridge to learn the connections between tokens. With the semantic similarity between tokens and concepts $\mathbf{S}$, the connection $\mathbf{a}_{i,j}$ between ith token and jth token is calculated by:

$$\mathbf{a}_{i,j} = \frac{\exp(\mathrm{sim}(\mathbf{S}_i, \mathbf{S}_j)/\tau)}{\sum_{j=1}^{N}\exp(\mathrm{sim}(\mathbf{S}_i, \mathbf{S}_j)/\tau)}, \tag{11}$$

where $\mathbf{S}_i$ is the semantic similarity between ith token and all concepts, and τ denote temperature parameter. Intuitively, tokens belonging to similar concepts are more likely to be connected with a higher probability. This approach offers two advantages compared to directly calculating connection probabilities based on token embeddings. Firstly, it mitigates potential noise connections caused by irrelevant features in high-dimensional embedding $\mathbf{t}$. Secondly, the graph structure constructed based on concepts related to biomarkers and radiological characteristics of the disease is more meaningful in neuroscience. Based on this, we treat the constructed graph structure $\mathbf{A}$ as the prompt for pre-trained foundation modal.

3.4.2. Graph embedding

After obtaining the constructed graph structure $\mathbf{A}$, we employ the widely-adopted GCN model as the graph encoder to obtain the graph embedding in this study. The GCN operation in lth GCN layer is formally defined as:

$$\mathcal{F}_{\mathrm{GCN}}(\mathbf{A}, \mathbf{H}) = \sigma(\tilde{\mathbf{D}}^{-\frac{1}{2}}\tilde{\mathbf{A}}\tilde{\mathbf{D}}^{-\frac{1}{2}}\mathbf{H}\boldsymbol{\Theta}), \tag{12}$$

where $\tilde{\mathbf{A}} = \mathbf{A} + \mathbf{I}$ is the adjacency matrix $\mathbf{A}$ with added self-connections through the identity matrix $\mathbf{I}$, $\tilde{\mathbf{D}}$ is the diagonal matrix of $\tilde{\mathbf{A}}$, $\mathbf{H}^{(l)}$ is the input embeddings of all nodes, $\boldsymbol{\Theta}$ is the trainable weight matrix, and $\sigma(\cdot)$ represents an activation function. Furthermore, the embeddings of all tokens with graph prompt can be expressed as:

$$\mathbf{T}^G = \mathcal{F}_{\mathrm{GCN}}(\mathbf{A}, \tilde{\mathbf{T}}), \tag{13}$$

where $\tilde{\mathbf{T}}$ is the weighted embeddings of the tokens. As a result, our method obtains the prompted token embeddings $\mathbf{T}^G$ by extracting the structural information among tokens to prompt the pre-trained fundation models. Furthermore, the prompted token embeddings $\mathbf{T}^G$ are fed into a unified transformer-based encoder $\mathcal{F}_{uni}(\cdot)$ to obtain the representation of the subject, *i.e.,* $\mathbf{z} = \mathcal{F}_{uni}(\mathbf{T}^G), \mathbf{z} \in \mathbb{R}^d$.

Finally, we produce a prediction of the subject by two functions, *i.e.,* concept project function $\phi : \mathbb{R}^d \to \mathbb{R}^{K\times C}$ and label project function $\mathcal{F}_y : \mathbb{R}^{K\times C} \to \mathcal{Y}$. In this way, we apply cross-entropy loss as the objective function, *i.e.,*

$$\mathcal{L}_{\mathrm{CE}} = -\frac{1}{N_l}\sum_{i=1}^{N_l}\mathbf{y}_i \log\left(\mathcal{F}_y\left(\phi\left(\mathbf{z}_i, \mathbf{Z}_{cpt}\right)\right)\right), \tag{14}$$

where $\mathbf{y} \in \mathcal{Y}$ denotes label, $\mathbf{Z}_{cpt}$ is the concept embeddings obtained from Eq. (8), and N_l is number of labeled subjects.

4. Experiments

4.1. Experimental settings

4.1.1. Datasets

We conduct experiments on two public multimodal neurological disorder datasets, *i.e.,* Alzheimer's Disease Neuroimaging Initiative (ADNI)[1] (Jack et al., 2008) and Autism brain imaging data exchange (ABIDE)[2] (Di Martino et al., 2014). The subjects are categorized into four groups in ADNI: NC (normal control), EMCI (early mild cognitive impairment), LMCI (late mild cognitive impairment), and AD (Alzheimer's disease). In total, we included 409 pairs of data (*i.e.,* NC /LMCI/AD for ADNI-3CLS) and 770 pairs of data (*i.e.,* NC/EMCI/LMCI /AD for ADNI-4CLS). The subjects are categorized into two groups in ABIDE: NC (normal control) and ASD (autism spectrum disorder) and we included 1029 pairs of data in ABIDE dataset.

We utilized the fslreorient2std, robustfov, FLIRT, and BET tools from the FSL software (Jenkinson et al., 2012) to preprocess data, the pipeline are follows. We first employed the fslreorient2std tool to reorient the images, aligning them with the orientation of the standard template image. Next, we utilized the robustfov tool to crop the MRI images, effectively removing the neck and lower jaw regions. The FLIRT tool (Jenkinson et al., 2002) was used to register all MRI images to the Colin27 template (Holmes et al., 1998), correcting for global linear differences and resampling the images to a consistent resolution ($1 \times 1 \times 1$ mm^3) and size ($191 \times 217 \times 191$). Finally, we applied the BET tool to remove the skull and dura mater.

4.1.2. Comparison methods

The comparison methods include one baseline transformer method (*i.e.,* ViT (Dosovitskiy et al., 2020)), two transformer-based methods for neurological disorders diagnosis (*i.e.,* BrainT (Kan et al., 2022) and GraphT (Cai et al., 2022)), two vanilla multimodal models (*i.e.,* CLIP (Radford et al., 2021) and MetaT (Zhang et al., 2023b)), and two prompt learning methods (*i.e.,* VPT (Jia et al., 2022) and MaPLe (Khattak et al., 2023)). We list the details of the comparison methods as follows:

- **ViT** is treated as a baseline method. ViT applies the core ideas of transformers to image classification tasks. It treats images as sequences of patches and processes them using self-attention mechanisms, setting a precedent for subsequent transformer-based models in computer vision.
- **BrainT** leverages the transformer to efficiently learn connection strengths between brain regions and incorporate an orthonormal clustering readout operation to capture functional modules within the brain.
- **GraphT** introduces a graph transformer framework that leverages multimodal neuroimaging data to improve Alzheimer's Disease diagnosis and brain age estimation by capturing complex cross-modal interactions and fusing them through geometric learning.
- **CLIP** is a multimodal model, which learns visual concepts from natural language supervision. It has been shown to be effective in a wide range of visual tasks by leveraging the power of language-image pre-training.
- **MetaT** introduces a unified approach to multimodal learning, employing a frozen encoder and a shared token space to process diverse data types without paired training data.
- **VPT** introduces efficient prompt learning to full fine-tuning for large-scale transformer models in computer vision. This groundbreaking methodology not only streamlines the training process but also significantly optimizes the utilization of computational resources.
- **MaPLe** introduces a multimodal prompt learning method that strategically masks parts of the input to guide the model towards more effective learning and adaptation to specific tasks, including those involving multi-modal data.

4.1.3. Implementation details

All experiments are conducted on a server with 8 NVIDIA GeForce 3090 GPU (24.0 GB caches). In our method, we utilize the text encoder and vision encoder from the pre-trained multimodal model BiomedCLIP (Zhang et al., 2023a) as the initial weights for our text encoder and unified encoder. Moreover, BiomedCLIP was trained on 15 million pairs of medical image–text data. By leveraging the pre-trained BERT model from BiomedCLIP, we are able to effectively align concept texts with embeddings that possess semantic meaning in the image space. To achieve efficient fine-tuning, the parameters of these encoders do

[1] https://adni.loni.usc.edu/.

[2] http://fcon_1000.projects.nitrc.org/indi/abide/.

Table 1
Diagnose performance (mean and standard deviation) of all methods on all datasets. Note that, “ADNI-3CLS” and “ADNI-4CLS” indicate the classification on three classes “NC/LMCI/AD” and the classification on four classes “NC/EMCI/LMCI/AD”, respectively.

Methods	ADNI-3CLS				
	ACC	AUC	SPE	SEN	F1
ViT	0.6707 ± 0.0387	0.6997 ± 0.0411	0.5837 ± 0.0332	0.5749 ± 0.0402	0.5749 ± 0.0323
BrainT	0.6504 ± 0.0640	0.6853 ± 0.0422	0.5589 ± 0.0358	0.5806 ± 0.0328	0.5692 ± 0.0353
GraphT	0.6911 ± 0.0744	0.7172 ± 0.0810	0.5729 ± 0.0580	0.5954 ± 0.0602	0.5757 ± 0.0440
CLIP	0.7073 ± 0.0467	0.7361 ± 0.0483	0.5671 ± 0.0383	0.6144 ± 0.0363	0.5869 ± 0.0376
MetaT	0.7114 ± 0.0365	0.7521 ± 0.0415	0.5674 ± 0.0303	0.6252 ± 0.0482	0.5944 ± 0.0368
VPT	0.7561 ± 0.0222	0.7891 ± 0.0272	0.6049 ± 0.0277	0.6627 ± 0.0293	0.6322 ± 0.0283
MaPLe	0.7805 ± 0.0345	0.8093 ± 0.0516	0.7272 ± 0.0497	0.6775 ± 0.0482	0.6708 ± 0.0356
MMGPL	0.8230 ± 0.0310	0.8514 ± 0.0172	0.7714 ± 0.0126	0.7314 ± 0.0412	0.7467± 0.0312
Methods	ADNI-4CLS				
	ACC	AUC	SPE	SEN	F1
ViT	0.3766 ± 0.0165	0.4530 ± 0.0179	0.3660 ± 0.0167	0.3631 ± 0.0161	0.3644 ± 0.0142
BrainT	0.4091 ± 0.0224	0.5859 ± 0.0210	0.4246 ± 0.0192	0.3680 ± 0.0196	0.3681 ± 0.0211
GraphT	0.3961 ± 0.0409	0.5188 ± 0.0373	0.3961 ± 0.0429	0.3388 ± 0.0387	0.3143 ± 0.0431
CLIP	0.4351 ± 0.0221	0.6013 ± 0.0230	0.4791 ± 0.0261	0.4077 ± 0.0305	0.4247 ± 0.0286
MetaT	0.4286 ± 0.0312	0.5779 ± 0.0347	0.4922 ± 0.0313	0.4061 ± 0.0226	0.4136 ± 0.0248
VPT	0.4416 ± 0.0303	0.6198 ± 0.0297	0.4455 ± 0.0252	0.4149 ± 0.0251	0.4219 ± 0.0295
MaPLe	0.4675 ± 0.0372	0.6357 ± 0.0275	0.4922 ± 0.0202	0.4641 ± 0.0288	0.4722 ± 0.0305
MMGPL	0.5159 ± 0.0184	0.6422 ± 0.0484	0.5252 ± 0.0308	0.4317 ± 0.0243	0.4779 ± 0.0179
Methods	ABIDE				
	ACC	AUC	SPE	SEN	F1
ViT	0.6463 ± 0.0443	0.6574 ± 0.0410	0.5216 ± 0.0501	0.5852 ± 0.0269	0.5888 ± 0.0279
BrainT	0.7073 ± 0.0402	0.7360 ± 0.0440	0.6769 ± 0.0219	0.6280 ± 0.0530	0.6463 ± 0.0376
GraphT	0.6585 ± 0.0215	0.6911 ± 0.0424	0.5507 ± 0.0372	0.5340 ± 0.0285	0.5523 ± 0.0279
CLIP	0.6707 ± 0.0416	0.6868 ± 0.0424	0.6313 ± 0.0518	0.5656 ± 0.0665	0.6035 ± 0.0377
MetaT	0.6585 ± 0.0228	0.6880 ± 0.0196	0.5737 ± 0.0472	0.5675 ± 0.0505	0.5761 ± 0.0465
VPT	0.6973 ± 0.0305	0.7363 ± 0.0356	0.6500 ± 0.0456	0.6267 ± 0.0426	0.6356 ± 0.0501
MaPLe	0.7195 ± 0.0326	0.7418 ± 0.0380	0.6682 ± 0.0232	0.6024 ± 0.0229	0.6580 ± 0.0319
MMGPL	0.7239 ± 0.0229	0.7540 ± 0.0485	0.6422 ± 0.0328	0.6897 ± 0.0272	0.6723 ± 0.0413

not need to be updated (*i.e.,* frozen) during the fine-tuning process. Furthermore, this ensures that the embeddings obtained from the text encoder and unified encoder are aligned with each other. Additionally, all parameters are initialized by the Glorot initialization and optimized by the AdamW optimizer with initial learning rate 0.0001, and decay it by 0.2 at epochs 30 and 60. MMGPL is trained with a fixed epoch 100. The patch size is set in the range of $\{16, 24, 32, 64\}$ and the batch size is set in the range of $\{4, 8, 16\}$ according to memory. We obtained the author-verified codes for all comparison methods and tune the parameters for all comparison methods as suggested in their published works. Furthermore, for methods that are originally single-modal, we adopt the results from the best-performing modality as the final outcome. In the case of BrainT, we replace its tokenizer module to adapt to the modality data utilized in the experiment.

We use 5-fold cross-validation in all experiments and repeat the experiments three times with random seeds. Finally, the average results and the corresponding standard deviation results (std) for each method are reported. All methods' results are evaluated using five metrics: Accuracy (ACC), Area Under the Receiver Operating Characteristic Curve (AUC), Specificity (SPE), Sensitivity (SEN), and F1-score (F1).

4.2. *Experimental results and analysis*

4.2.1. *Diagnose performance*

Table 1 summarizes the diagnose performances of all methods on all datasets. From the experimental results, we could have the following conclusions.

Firstly, the proposed MMGPL performs comparably or significantly better than the state-of-the-art methods. For example, compared to one of the best competitors (*e.g.,* MaPLe), MMGPL averagely improves by about 7.1% on ADNI-3CLS, 2.1% on ADNI-4CLS, and 3.0% on ABIDE, respectively. Moreover, compared to one of the baseline competitors (*e.g.,* MetaT), MMGPL averagely improves by about 21.4% on ADNI-3CLS, 12.0% on ADNI-4CLS, and 13.9% on ABIDE, respectively. These results validate the effectiveness of our method. The possible reasons can be that we reduce the weight of irrelevant patches and incorporate a graph prompt to extract structural information among patches, making our method particularly suitable for neurological disorders diagnosis.

Secondly, among all methods, methods that utilize pre-trained large models (*e.g.,* CLIP, MetaT, VPT, MaPLe, and MMGPL) outperform other methods trained directly on the dataset (*e.g.,* ViT, BrainT, and GraphT). For example, compared to ViT, BrainT, and GraphT, MMGPL averagely improves by about 25.2% on ADNI-3CLS, 31.3% on ADNI-4CLS, and 16.5% on ABIDE, respectively. The superior performance of pre-trained models can be attributed to their exposure to a diverse range of tasks during pre-training, which enhances their ability to generalize to new tasks. This advantage is particularly beneficial when dealing with relatively small target datasets, as is frequently encountered in neurological disorder diagnosis.

Thirdly, among all methods, methods that utilize prompt learning techniques (*e.g.,* VPT, MaPLe, and MMGPL) outperform the vanilla turning method on pre-trained large models (*e.g.,* CLIP and MetaT). For example, compared to CLIP and MetaT, MMGPL averagely improves by about 24.5% on ADNI-3CLS, 11.2% on ADNI-4CLS, and 9.5% on ABIDE, respectively. The possible reason for this is that prompt learning typically involves tuning a small set of parameters that guide the model to apply its pre-learned knowledge in a specific and task-relevant manner.

4.2.2. *Ablation studies*

We further conduct the ablation studies with individual components and report their results in Fig. 2. Specifically, “B” denotes the baseline method which applies the fine-turning strategy introduced in method MetaT (Zhang et al., 2023b). Based on this, we apply concept learning (*i.e.,* Section 3.3) to reduce the weights of irrelevant patches and denote as “B+W”. Similarly, we employ graph prompt learning (*i.e.,* Section 3.4) and denote as “B+G”. Note that, in order to ensure the

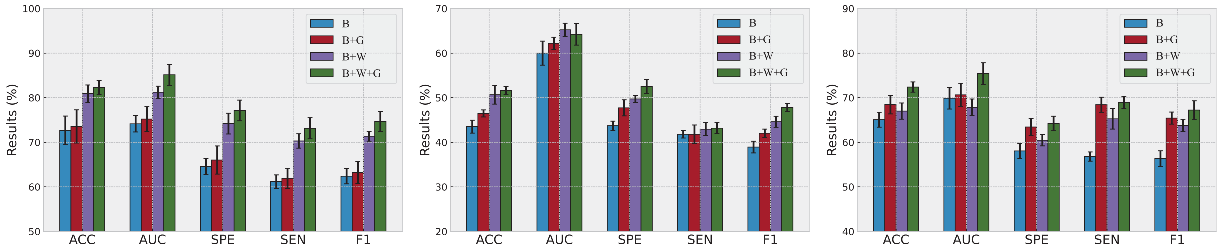

(a) ADNI-3CLS (b) ADNI-4CLS (c) ABIDE

Fig. 2. Performance of MMGPL with different combinations of components on all datasets, *i.e.,* "B" denotes baseline method, "B+G" denotes baseline method with graph prompt learning, "B+W" denotes baseline method with token weights, and "B+W+G" denotes baseline method with graph prompt learning and token weights.

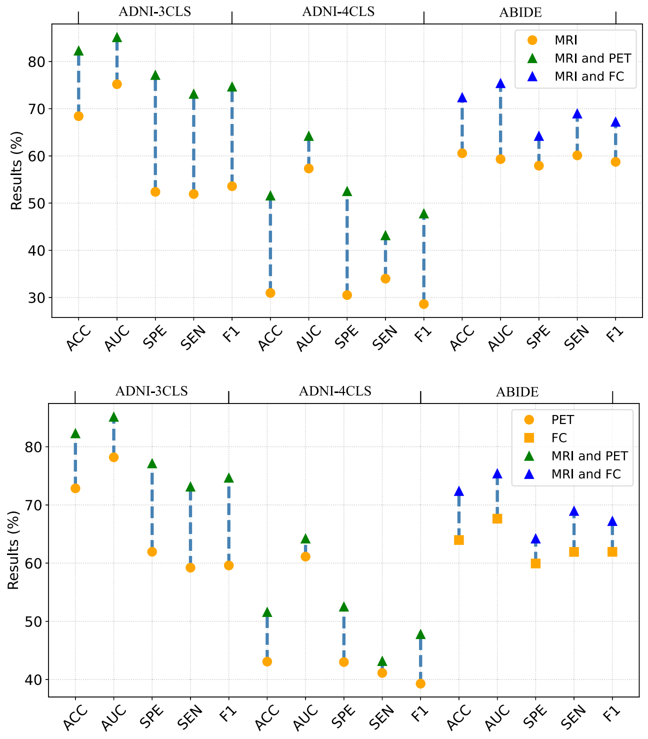

Fig. 3. Performance of MMGPL with different modalities.

proper running of the method, the semantic similarity is still needed to calculate in method "B+G". Moreover, we involve both token weights and graph prompt learning which denotes as "B+W+G".

Based on the experimental results, we could observe that each component has a contribution. In particular, compared to the baseline method "B", the method "B+G" averagely improves by 5.3%. Moreover, the method "B+W" markedly outperforms that of the baseline method "B". Hence, the proposed concept learning and graph prompt learning modules have a positive effect on the diagnosis of neurological disorders, which verified our claim that reduces the weight of irrelevant patches and incorporates a graph prompt making our method particularly suitable for neurological disorders diagnosis. Besides, we observed that concept learning with token weights contributes more significantly to the overall performance compared to graph prompts. One possible reason is that without token weights, the inclusion of many irrelevant tokens during graph prompt learning could have a negative impact. Considering the message propagation mechanism of GCN, these irrelevant tokens can potentially affect the graph prompt learning process and consequently affect the overall performance. Therefore, the two modules, concept learning with token weights and graph prompt learning, are closely intertwined and mutually dependent on each other.

Table 2
Comparison between MMGPL and related works on scalability. Note that, ✓(vanilla) indicates can only supports two modalities and is challenging to expand to supports more modalities.

Method	Multiple modalities	Unified model	Prompt
ViT		✓	
BrainT		✓	
GraphT	✓(vanilla)		
CLIP	✓(vanilla)		
MetaT	✓	✓	
VPT		✓	✓
MaPLe	✓(vanilla)		✓
MMGPL	✓	✓	✓

4.2.3. Analysis

Multi-modalities. We investigate the effectiveness of individual modalities and multi-modalities by reporting the performances in Fig. 3. Concretely, our method considering multi-modalities (*e.g.,* MRI and PET in ADNI) obtains substantial improvements across all metrics, compared to only considering individual modalities. This suggests that the complementary information captured by different modalities can enhance the overall performance of the model.

Interpretability. We further investigate the interpretability of our method. To achieve this, we scale the heat maps and superimpose them on the corresponding positions of the original images. Note that, the heat maps are generated based on token weights. The visualization of the heat map is presented in Fig. 4, with darker shades of red signifying higher weights and darker shades of blue signifying lower weights. Specifically, the x-axis represents different positions within the same plane, while the y-axis represents different planes. Firstly, it is evident that our method effectively eliminates the weights associated with almost all irrelevant patches. Secondly, Fig. 4 indicates that our method is capable of identifying the critical regions within the brain, such as hippocampal and parahippocampal. Moreover, its interpretability has been validated by clinicians.

Scalability. We further conduct a comparison between MMGPL and related works in terms of scalability. As shown in Table 2. we evaluate three aspects of scalability, *i.e.,* multiple modalities, unified model, and prompt. In particular, considering the inherent multimodality of medical data, we first evaluate the model's ability to handle multiple modalities. Note that, ✓(vanilla) indicates can only support two modalities (*e.g.,* image and text) and is challenging to expand to support more modalities. Secondly, we evaluate whether the method applies a unified model for encoding multimodal medical imaging, as employing a unified model facilitates efficient inference and deployment. Thirdly, we evaluate whether the method applies prompt for fine-turning, as prompt-driven fine-turning is beneficial for enhancing the interactivity and effectiveness of the method. Comparing MMGPL with all comparison methods, we can observe that our method achieves better scalability and flexibility.

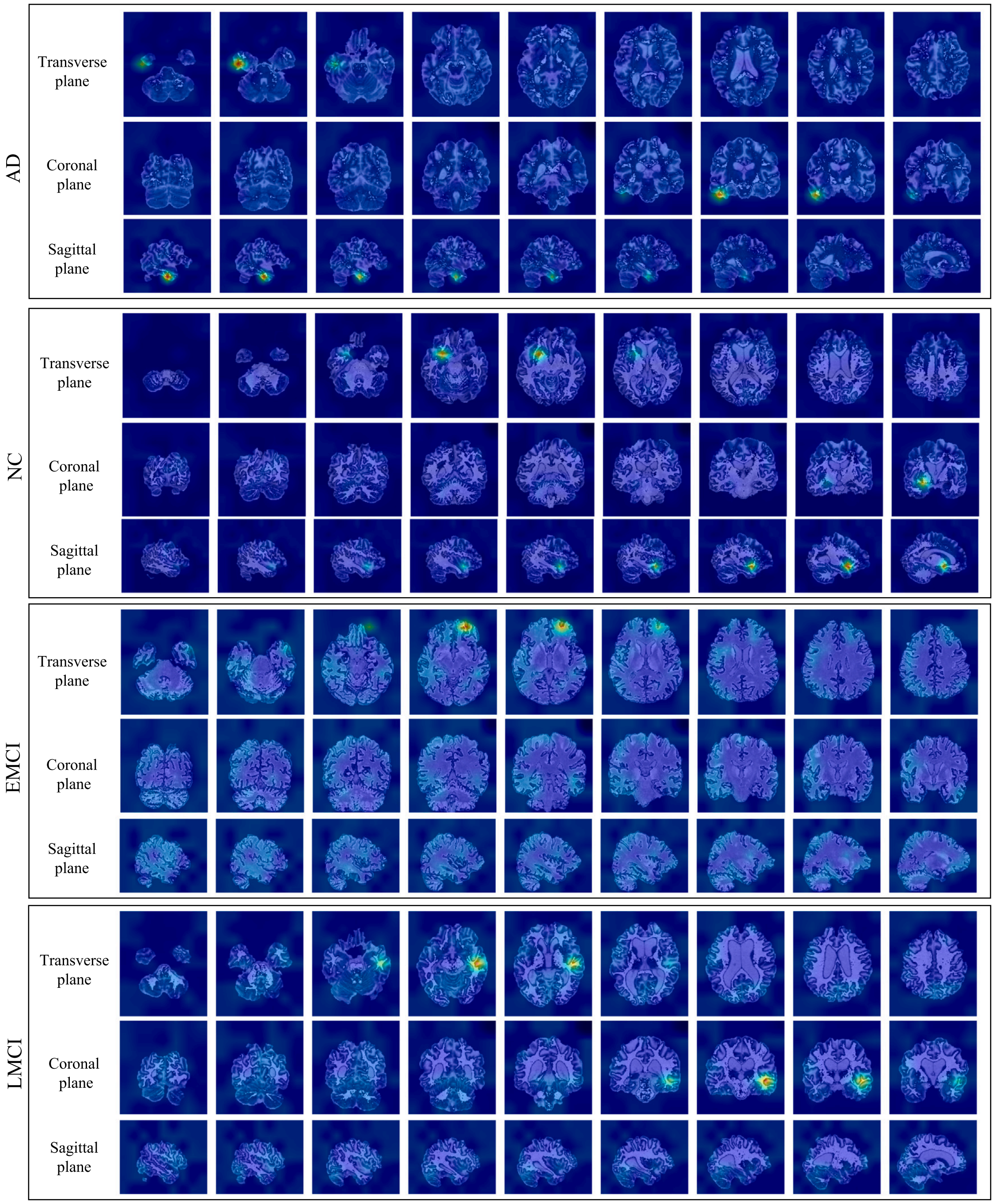

Fig. 4. Heat maps generated by MMGPL on different subjects in ADNI dataset.

Semantic similarity graph. To improve the interpretability of MMGPL, we visualize the semantic similarity graph of samples belonging to different classes in Fig. 5. Specifically, the semantic similarity graph is sparse. The reason could be that those concepts naturally have low similarity or limited overlap. Moreover, sparse semantic similarity graphs are easier to interpret as they highlight the most significant concepts. For example, in the middle sub-figure, the model infers the sample as LMCI category based on the fifth concept.

Concept weights. To quantify the weights of concepts, we conducted a statistical analysis on the number of times concepts were activated by samples belonging to different classes, and visualized the results using the Sankey diagram in Fig. 6. Firstly, the weights of concepts can accurately represent their corresponding categories. In the top side of Fig. 6, it can be observed that the top four concepts, which represent NC-related concepts, have the highest probability of being activated in NC samples. Moreover, concepts related to hippocampal atrophy tend to have higher weights and proportions in both LMCI and AD categories. This finding aligns with prior knowledge that hippocampal atrophy is associated with cognitive decline in patients with LMCI and AD. Secondly, There may be instances where samples from one category activate concepts belonging to other categories. For example, LMCI samples might activate concepts associated with the NC category. This could be due to individual variations, where pathological samples may not satisfy all the concepts. It is worth noting that NC samples rarely

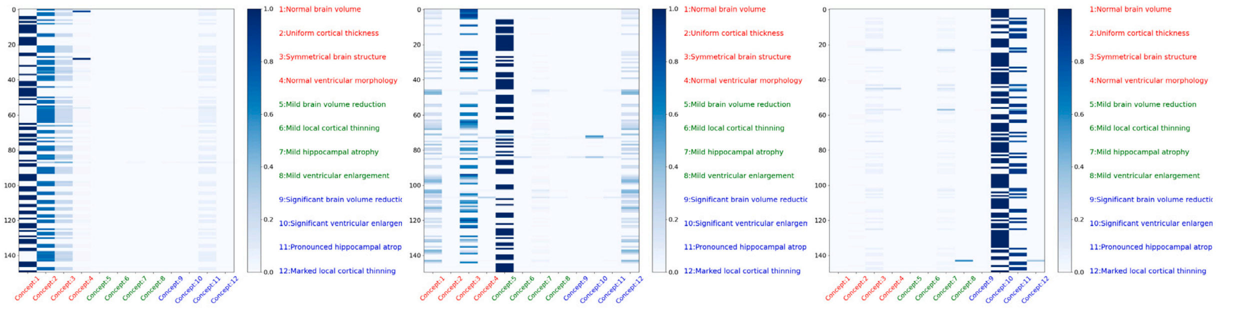

(a) NC (b) LMCI (c) AD

Fig. 5. The visualization of concept-similarity graph on the ADNI dataset. The horizontal and vertical axes represent concepts and tokens. Different colors represent concepts belonging to different categories. The red texts represent concepts related to NC, the green texts represent concepts related to LMCI, and the blue texts represent concepts related to AD.

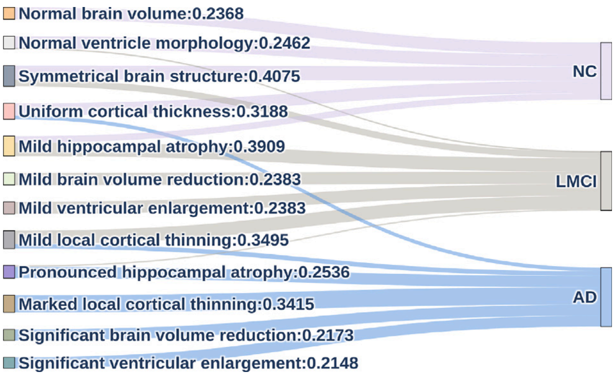

Fig. 6. The visualization of the quantified impact of different concepts on the ADNI dataset. The concepts are shown on the left side, while classes are shown on the right side. The width of the lines corresponds to the magnitude of the weights, and the values indicate the specific weight values.

activate concepts related to AD, while AD samples may activate concepts associated with NC. This finding aligns with clinical expectations, as NC samples typically do not exhibit any AD-related symptoms. However, some AD samples may still satisfy some concepts associated with NC. Moreover, LMCI samples can originate from concepts related to both NC and AD. This finding aligns with clinical expectations, as LMCI represents an intermediate state between NC and AD.

5. Conclusion

In this paper, we proposed a graph prompt learning fine-turning framework for neurological disorder diagnosis, by jointly considering the impact of irrelevant patches as well as the structural information among tokens in multimodal medical data. Specifically, we conduct concept learning, aiming to reduce the weights of irrelevant tokens according to the semantic similarity between each token and disease-related concepts. Moreover, we conducted graph prompt learning with concept embeddings, aiming to bridge the gap between multimodal models and neurological disease diagnosis. Experimental results demonstrated the effectiveness of our proposed method, compared to state-of-the-art methods on neurological disease diagnosis tasks.

CRediT authorship contribution statement

Liang Peng: Writing – original draft, Visualization, Validation, Supervision, Software, Project administration, Methodology, Investigation, Formal analysis, Conceptualization. **Songyue Cai:** Visualization, Validation, Software, Methodology, Investigation, Data curation, Conceptualization. **Zongqian Wu:** Validation, Methodology, Investigation, Formal analysis, Conceptualization. **Huifang Shang:** Supervision, Resources, Methodology, Investigation, Funding acquisition, Formal analysis, Data curation. **Xiaofeng Zhu:** Writing – original draft, Supervision, Resources, Project administration, Methodology, Investigation, Funding acquisition, Formal analysis, Conceptualization. **Xiaoxiao Li:** Writing – original draft, Supervision, Resources, Methodology, Investigation, Formal analysis, Conceptualization.

Declaration of competing interest

The authors declare that they have no known competing financial interests or personal relationships that could have appeared to influence the work reported in this paper.

Data availability

The authors do not have permission to share data.

Declaration of Generative AI and AI-assisted technologies in the writing process

During the preparation of this work the author(s) used GPT-4 in order to improve language and readability. After using this tool/service, the author(s) reviewed and edited the content as needed and take(s) full responsibility for the content of the publication.

Acknowledgments

This work was supported in part by National Key Research and Development Program of China under Grant No. 2022YFA1004100 and Natural Science Foundation of Guangdong Province of China under Grant 2024A1515011381.

References

Belmonte, M.K., Allen, G., Beckel-Mitchener, A., Boulanger, L.M., Carper, R.A., Webb, S.J., 2004. Autism and abnormal development of brain connectivity. J. Neurosci. 24 (42), 9228–9231.

Bessadok, A., Mahjoub, M.A., Rekik, I., 2022. Graph neural networks in network neuroscience. IEEE Trans. Pattern Anal. Mach. Intell. 45 (5), 5833–5848.

Brown, T., Mann, B., Ryder, N., Subbiah, M., Kaplan, J.D., Dhariwal, P., Neelakantan, A., Shyam, P., Sastry, G., Askell, A., 2020. Language models are few-shot learners. Adv. Neural Inf. Process. Syst. 33, 1877–1901.

Bullmore, E., Sporns, O., 2009. Complex brain networks: graph theoretical analysis of structural and functional systems. Nat. Rev. Neurosci. 10 (3), 186–198.

Cai, H., Gao, Y., Liu, M., 2022. Graph transformer geometric learning of brain networks using multimodal MR images for brain age estimation. IEEE Trans. Med. Imaging 42 (2), 456–466.

Devlin, J., Chang, M.-W., Lee, K., Toutanova, K., 2018. Bert: Pre-training of deep bidirectional transformers for language understanding. arXiv preprint arXiv:1810.04805.

Di Martino, A., Yan, C.-G., Li, Q., Denio, E., Castellanos, F.X., Alaerts, K., Anderson, J.S., Assaf, M., Bookheimer, S.Y., Dapretto, M., 2014. The autism brain imaging data exchange: towards a large-scale evaluation of the intrinsic brain architecture in autism. Mol. Psychiatry 19 (6), 659–667.

Dinsdale, N.K., Bluemke, E., Sundaresan, V., Jenkinson, M., Smith, S.M., Namburete, A.I., 2022. Challenges for machine learning in clinical translation of big data imaging studies. Neuron.

Dosovitskiy, A., Beyer, L., Kolesnikov, A., Weissenborn, D., Zhai, X., Unterthiner, T., Dehghani, M., Minderer, M., Heigold, G., Gelly, S., 2020. An image is worth 16x16 words: Transformers for image recognition at scale. arXiv preprint arXiv:2010.11929.

Driess, D., Xia, F., Mehdi, S., Sajjadi, C., Lynch, A., Chowdhery, B., Ichter, A., Wahid, J., Tompson, Q., Vuong, T., Yu, W., Huang, Y., Chebotar, P., Sermanet, D., Duckworth, S., Levine, V., Vanhoucke, K., Hausman, M., Toussaint, K., Greff, A., Zeng, I., Mordatch, P., Florence, 2023. Palm-e: An embodied multimodal language model. arXiv:arXiv:2303.03378.

Dvornek, N.C., Li, X., Zhuang, J., Duncan, J.S., 2019. Jointly discriminative and generative recurrent neural networks for learning from fMRI. In: MLMI. Springer, pp. 382–390.

Feigin, V.L., Vos, T., Nichols, E., Owolabi, M.O., Carroll, W.M., Dichgans, M., Deuschl, G., Parmar, P., Brainin, M., Murray, C., 2020. The global burden of neurological disorders: translating evidence into policy. Lancet Neurol. 19 (3), 255–265.

Fornito, A., Zalesky, A., Breakspear, M., 2015. The connectomics of brain disorders. Nat. Rev. Neurosci. 16 (3), 159–172.

Gao, T., Fisch, A., Chen, D., 2020. Making pre-trained language models better few-shot learners. arXiv preprint arXiv:2012.15723.

Girdhar, R., El-Nouby, A., Liu, Z., Singh, M., Alwala, K.V., Joulin, A., Misra, I., 2023. Imagebind: One embedding space to bind them all. In: Proceedings of the IEEE/CVF Conference on Computer Vision and Pattern Recognition. pp. 15180–15190.

Holmes, C.J., Hoge, R., Collins, L., Woods, R., Toga, A.W., Evans, A.C., 1998. Enhancement of MR images using registration for signal averaging. J. Comput. Assist. Tomogr. 22 (2), 324–333.

Holzinger, A., Malle, B., Saranti, A., Pfeifer, B., 2021. Towards multi-modal causability with graph neural networks enabling information fusion for explainable AI. Inf. Fusion 71, 28–37.

Howard, J., Ruder, S., 2018. Universal language model fine-tuning for text classification. In: Gurevych, I., Miyao, Y. (Eds.), Proceedings of the 56th Annual Meeting of the Association for Computational Linguistics (Volume 1: Long Papers). pp. 328–339. http://dx.doi.org/10.18653/v1/P18-1031.

Huang, Y., Yang, X., Liu, L., Zhou, H., Chang, A., Zhou, X., Chen, R., Yu, J., Chen, J., Chen, C., 2023. Segment anything model for medical images? arXiv preprint arXiv:2304.14660.

Jack, Jr., C.R., Bernstein, M.A., Fox, N.C., Thompson, P., Alexander, G., Harvey, D., Borowski, B., Britson, P.J., L. Whitwell, J., Ward, C., 2008. The Alzheimer's disease neuroimaging initiative (ADNI): MRI methods. J. Magn. Reson. Imaging: Off. J. Int. Soc. Magn. Reson. Med. 27 (4), 685–691.

Jaszczur, S., Chowdhery, A., Mohiuddin, A., Kaiser, L., Gajewski, W., Michalewski, H., Kanerva, J., 2021. Sparse is enough in scaling transformers. Adv. Neural Inf. Process. Syst. 34, 9895–9907.

Jenkinson, M., Bannister, P., Brady, M., Smith, S., 2002. Improved optimization for the robust and accurate linear registration and motion correction of brain images. Neuroimage 17 (2), 825–841.

Jenkinson, M., Beckmann, C.F., Behrens, T.E., Woolrich, M.W., Smith, S.M., 2012. Fsl. Neuroimage 62 (2), 782–790.

Jia, M., Tang, L., Chen, B.-C., Cardie, C., Belongie, S., Hariharan, B., Lim, S.-N., 2022. Visual prompt tuning. In: European Conference on Computer Vision. Springer, pp. 709–727.

Kan, X., Dai, W., Cui, H., Zhang, Z., Guo, Y., Yang, C., 2022. Brain network transformer. Adv. Neural Inf. Process. Syst. 35, 25586–25599.

Kazi, A., Shekarforoush, S., Krishna, S.A., Burwinkel, H., Vivar, G., Kortüm, K., Ahmadi, S.-A., Albarqouni, S., Navab, N., 2019. Inceptiongcn: receptive field aware graph convolutional network for disease prediction. In: IPMI. Springer, pp. 73–85.

Khattak, M.U., Rasheed, H., Maaz, M., Khan, S., Khan, F.S., 2023. Maple: Multi-modal prompt learning. In: Proceedings of the IEEE/CVF Conference on Computer Vision and Pattern Recognition. pp. 19113–19122.

Kipf, T.N., Welling, M., 2017. Semi-supervised classification with graph convolutional networks. pp. 1–14,

Kirillov, A., Mintun, E., Ravi, N., Mao, H., Rolland, C., Gustafson, L., Xiao, T., Whitehead, S., Berg, A.C., Lo, W.-Y., 2023. Segment anything. arXiv preprint arXiv:2304.02643.

Koh, P.W., Nguyen, T., Tang, Y.S., Mussmann, S., Pierson, E., Kim, B., Liang, P., 2020. Concept bottleneck models. In: International Conference on Machine Learning. PMLR, pp. 5338–5348.

LeCun, Y., Bengio, Y., 1995. Convolutional networks for images, speech, and time series. In: The Handbook of Brain Theory and Neural Networks. Vol. 3361, 1995.

Lester, B., Al-Rfou, R., Constant, N., 2021. The power of scale for parameter-efficient prompt tuning. arXiv preprint arXiv:2104.08691.

Li, X.L., Liang, P., 2021. Prefix-tuning: Optimizing continuous prompts for generation. arXiv preprint arXiv:2101.00190.

Li, C., Wong, C., Zhang, S., Usuyama, N., Liu, H., Yang, J., Naumann, T., Poon, H., Gao, J., 2023. Llava-med: Training a large language-and-vision assistant for biomedicine in one day. arXiv preprint arXiv:2306.00890.

Li, X., Zhou, Y., Dvornek, N., Zhang, M., Gao, S., Zhuang, J., Scheinost, D., Staib, L.H., Ventola, P., Duncan, J.S., 2021. Braingnn: Interpretable brain graph neural network for fmri analysis. Med. Image Anal. 74, 102233.

Liu, X., Ji, K., Fu, Y., Tam, W., Du, Z., Yang, Z., Tang, J., 2022. P-tuning: Prompt tuning can be comparable to fine-tuning across scales and tasks. In: Proceedings of the 60th Annual Meeting of the Association for Computational Linguistics. pp. 61–68.

Liu, H., Li, C., Wu, Q., Lee, Y.J., 2023. Visual instruction tuning. In: NeurIPS.

Lord, C., Elsabbagh, M., Baird, G., Veenstra-Vanderweele, J., 2018. Autism spectrum disorder. Lancet 392 (10146), 508–520.

Lu, Y., Liu, J., Zhang, Y., Liu, Y., Tian, X., 2022. Prompt distribution learning. In: Proceedings of the IEEE/CVF Conference on Computer Vision and Pattern Recognition. pp. 5206–5215.

Ma, J., Wang, B., 2023. Segment anything in medical images. arXiv preprint arXiv:2304.12306.

Maaz, M., Rasheed, H., Khan, S., Khan, F.S., 2023. Video-ChatGPT: Towards detailed video understanding via large vision and language models. arXiv preprint arXiv:2306.05424.

Miyai, A., Yu, Q., Irie, G., Aizawa, K., 2024. Locoop: Few-shot out-of-distribution detection via prompt learning. Adv. Neural Inf. Process. Syst. 36.

OpenAI, R., 2023. Gpt-4 Technical Report. Vol. 2, p. 13, arxiv:2303.08774. View Article.

Padurariu, M., Ciobica, A., Mavroudis, I., Fotiou, D., Baloyannis, S., 2012. Hippocampal neuronal loss in the CA1 and CA3 areas of Alzheimer's disease patients. Psychiatr. Danub. 24 (2.), 152–158.

Parisot, S., Ktena, S.I., Ferrante, E., Lee, M., Guerrero, R., Glocker, B., Rueckert, D., 2018. Disease prediction using graph convolutional networks: application to autism spectrum disorder and Alzheimer's disease. Med. Image Anal. 48, 117–130.

Pievani, M., Filippini, N., Van Den Heuvel, M.P., Cappa, S.F., Frisoni, G.B., 2014. Brain connectivity in neurodegenerative diseases—from phenotype to proteinopathy. Nat. Rev. Neurol. 10 (11), 620–633.

Radford, A., Kim, J.W., Hallacy, C., Ramesh, A., Goh, G., Agarwal, S., Sastry, G., Askell, A., Mishkin, P., Clark, J., 2021. Learning transferable visual models from natural language supervision. In: International Conference on Machine Learning. PMLR, pp. 8748–8763.

Rubinov, M., Sporns, O., 2010. Complex network measures of brain connectivity: uses and interpretations. Neuroimage 52 (3), 1059–1069.

Scheltens, P., De Strooper, B., Kivipelto, M., Holstege, H., Chételat, G., Teunissen, C.E., Cummings, J., van der Flier, W.M., 2021. Alzheimer's disease. Lancet 397 (10284), 1577–1590.

Schick, T., Schütze, H., 2020. Few-shot text generation with pattern-exploiting training. arXiv preprint arXiv:2012.11926.

Schuster, M., Paliwal, K.K., 1997. Bidirectional recurrent neural networks. IEEE Trans. Signal Process. 45 (11), 2673–2681.

Sun, L., Huang, Y., Wang, H., Wu, S., Zhang, Q., Gao, C., Huang, Y., Lyu, W., Zhang, Y., Li, X., et al., 2024. Trustllm: Trustworthiness in large language models. arXiv preprint arXiv:2401.05561.

Sun, Z., Yin, H., Chen, H., Chen, T., Cui, L., Yang, F., 2020. Disease prediction via graph neural networks. IEEE J. Biomed. Health Inf. 25 (3), 818–826.

Tsimpoukelli, M., Menick, J., Cabi, S., Eslami, O., Vinyals, F., Hill, 2021. Multimodal few-shot learning with frozen language models. arXiv:arXiv:2106.13884.

Tu, T., Azizi, S., Driess, D., Schaekermann, M., Amin, M., Chang, P.-C., Carroll, A., Lau, C., Tanno, R., Ktena, I., 2023. Towards generalist biomedical AI. arXiv preprint arXiv:2307.14334.

Vaswani, A., Shazeer, N., Parmar, N., Uszkoreit, J., Jones, L., Gomez, A.N., Kaiser, Ł., Polosukhin, I., 2017. Attention is all you need. Adv. Neural Inf. Process. Syst. 30.

Veličković, P., Cucurull, G., Casanova, A., Romero, A., Lio, P., Bengio, Y., 2017. Graph attention networks. arXiv preprint arXiv:1710.10903.

Wang, B., Li, L., Nakashima, Y., Nagahara, H., 2023. Learning bottleneck concepts in image classification. In: Proceedings of the IEEE/CVF Conference on Computer Vision and Pattern Recognition. pp. 10962–10971.

Wang, L., Zang, Y., He, Y., Liang, M., Zhang, X., Tian, L., Wu, T., Jiang, T., Li, K., 2006. Changes in hippocampal connectivity in the early stages of Alzheimer's disease: evidence from resting state fMRI. Neuroimage 31 (2), 496–504.

Wen, J., Thibeau-Sutre, E., Diaz-Melo, M., Samper-González, J., Routier, A., Bottani, S., Dormont, D., Durrleman, S., Burgos, N., Colliot, O., 2020. Convolutional neural networks for classification of Alzheimer's disease: Overview and reproducible evaluation. Med. Image Anal. 63, 101694.

Wingo, A.P., Liu, Y., Gerasimov, E.S., Gockley, J., Logsdon, B.A., Duong, D.M., Dammer, E.B., Robins, C., Beach, T.G., M, R.E., 2021. Integrating human brain proteomes with genome-wide association data implicates new proteins in Alzheimer's disease pathogenesis. Nat. Genet. 53 (2), 143–146.

Wu, C., Zhang, X., Zhang, Y., Wang, Y., Xie, W., 2023. Towards generalist foundation model for radiology. arXiv preprint arXiv:2308.02463.

Xu, H., Zhang, J., Wang, Z., Zhang, S., Bhalerao, M., Liu, Y., Zhu, D., Wang, S., 2023. GraphPrompt: Graph-based prompt templates for biomedical synonym prediction. In: Proceedings of the AAAI Conference on Artificial Intelligence. Vol. 37, pp. 10576–10584.

Yan, A., Wang, Y., Zhong, Y., He, Z., Karypis, P., Wang, Z., Dong, C., Gentili, A., Hsu, C.-N., Shang, J., et al., 2023. Robust and interpretable medical image classifiers via concept bottleneck models. arXiv preprint arXiv:2310.03182.

Yang, Y., Panagopoulou, A., Zhou, S., Jin, D., Callison-Burch, C., Yatskar, M., 2023. Language in a bottle: Language model guided concept bottlenecks for interpretable image classification. In: Proceedings of the IEEE/CVF Conference on Computer Vision and Pattern Recognition. pp. 19187–19197.

Zhang, Y., Gong, K., Zhang, K., Li, H., Qiao, Y., Ouyang, W., Yue, X., 2023b. Meta-transformer: A unified framework for multimodal learning. arXiv preprint arXiv:2307.10802.

Zhang, S., Metaxas, D., 2023. On the challenges and perspectives of foundation models for medical image analysis. arXiv preprint arXiv:2306.05705.

Zhang, S., Xu, Y., Usuyama, N., Xu, H., Bagga, J., Tinn, R., Preston, S., Rao, R., Wei, M., Valluri, N., et al., 2023a. BiomedCLIP: a multimodal biomedical foundation model pretrained from fifteen million scientific image-text pairs. arXiv preprint arXiv:2303.00915.

Zhang, Y., Zhou, T., Wang, S., Liang, P., Zhang, Y., Chen, D.Z., 2023c. Input augmentation with sam: Boosting medical image segmentation with segmentation foundation model. In: MICCAI. Springer, pp. 129–139.

Zheng, Q., Zhao, W., Wu, C., Zhang, X., Zhang, Y., Wang, Y., Xie, W., 2023. Large-scale long-tailed disease diagnosis on radiology images. arXiv preprint arXiv:2312.16151.

Zhou, K., Yang, J., Loy, C.C., Liu, Z., 2022. Conditional prompt learning for vision-language models. In: Proceedings of the IEEE/CVF Conference on Computer Vision and Pattern Recognition. pp. 16816–16825.

Zhu, Y., Ma, J., Yuan, C., Zhu, X., 2022. Interpretable learning based dynamic graph convolutional networks for Alzheimer's disease analysis. Inf. Fusion 77, 53–61.